International Journal of Biological Macromolecules 162 (2020) 1605–1615

Contents lists available at ScienceDirect

International Journal of Biological Macromolecules

journal homepage: http://www.elsevier.com/locate/ijbiomac

Natural polysaccharide derived carbon dot based in situ facile green synthesis of silver nanoparticles: Synergistic effect on breast cancer

Krishanu Ghosal [1], Santanu Ghosh [1], Debjani Ghosh, Kishor Sarkar *

Gene Therapy and Tissue Engineering Lab, Department of Polymer Science and Technology, University of Calcutta, 92, A.P.C. Road, Kolkata 700009, India

ARTICLE INFO

Article history:
Received 25 April 2020
Received in revised form 26 July 2020
Accepted 27 July 2020
Available online 02 August 2020

Keywords:
Carbon dot
Silver nanoparticles
Anticancer agent
Reactive oxygen species
Apoptosis

ABSTRACT

Over the decades, several nanoparticles have been developed for biomedical applications, still facile green synthesis derived nanoparticles showed tremendous attraction due to avoid of toxic solvent, ease of synthesis and low cost. Here, facile one pot in situ green synthesis is reported to develop silver nanoparticles with the aid of natural polysaccharide presented in sweet lemon peel waste derived carbon dot (CD) acted as a reducing and stabilizing agent at room temperature. The synthesis of CD and CD based silver nanoparticles (CD@AgNPs) was characterized by FTIR, UV–vis spectroscopy, fluorescence spectrophotometer, XRD and TEM. CD@AgNPs exhibited excellent antimicrobial activity against *E. coli* at very low concentration of 5.0 μg/ml. Interestingly, CD showed selective cytotoxicity against MCF7 breast cancer cells with the IC_{50} of 10 μg/ml while CD@AgNPs demonstrated synergistic effect on cytotoxicity. It is found that the cells death of MCF7 cells mainly occurred through the up-regulation of intracellular reactive oxygen species (ROS). Therefore, the synthesized CD@AgNPs may show an efficient anticancer agent for targeted breast cancer therapy in future.

© 2020 Elsevier B.V. All rights reserved.

1. Introduction

Over the last couple of years, nanoparticles have shown tremendous attraction in cancer research due to its smaller size ranging from 1 to 100 nm and high surface area (1000 m^2/g) [1]. Recent studies showed potential effect of nanoparticles as an anticancer agent on cancer tumor tissues due to its superior permeability and retention in tumor site because of its leaky vasculature and reduced lymphatic drainage [2–5]. Till date, a wide variety of nanoparticles have been investigated as potential anticancer agent like lipid based nanoparticles, polymer based nanocarriers, inorganic nanoparticles etc. [6,7] Despite the development of several anticancer agents for cancer therapy, efficient and targeted anticancer agents with low toxicity toward normal cells are still demanding. Owing to favourable optical properties along with biocompatibility, chemical stability, non-blinking and low level of toxicity carbon dots (CD) have shown immense attention for biomedical field [7–10]. Various procedures including laser ablation [11], electrochemical oxidation [12], microwave irradiation [13], ultrasonic [14] and solvothermal or hydrothermal technique [8,15]. Most of these techniques either consist toxic chemical or complicated reaction set up. In comparison, hydrothermal technique utilizes water as solvent and simple low cost reactor i.e. facile green synthesis which demands for biomedical application. In this context from last couple of years, researchers are working on the synthesis of fluorescent CD by using inexpensive renewable precursors and simple preparation method without using any organic chemical [16,17]. Till date, CD has been synthesized from many natural resources such as eutrophic algal blooms [18], watermelon peel [19], banana juice [20], orange juice [21], papaya [22], tulsi leaves [23], sweet potato [24], garlic [16], ginger [25], onion wastes [26], honey [27], aloe vera [28], gram-shells [29], etc. In a recent study [30], fresh tender ginger derived CD showed selective cellular toxicity toward human hepatocellular carcinoma cells (HepG2) where IC_{50} (50% inhibiting concentration) was at the concentration of 350 μg/ml. In another study [31], the IC_{50} of CD obtained from green tea was at the concentration of 150 μg/ml against MCF7 cells (breast cancer cells) and that of in MDA-MB-231 cells (triple negative breast cancer cells) was 72 μg/ml whereas the CD did not show any toxicity toward MCF-10A normal cells (non-tumorigenic epithelial cell line) even at higher concentration of 270 μg/ml. Although, the toxicity is greatly dependent of CD source and the actual reason behind the specificity to the various cancer cells still remains unknown. Therefore, it is hypothesized that CD may be an attractive anticancer material for cancer therapy.

Over the past few years, silver nanoparticles (AgNPs) have shown tremendous attraction toward biomedical field due to its severe antimicrobial activity [32], anti-inflammatory effect [33] and anti-cancer activity [34]. Recently, Zielinska et al. [35] showed that AgNPs caused the death of pancreatic cancer cells through programmed cell death mechanism i.e. apoptosis pathway although it was dependent upon particle size and the concentration of AgNPs. Similar mechanism also proposed

* Corresponding author.
E-mail address: kspoly@caluniv.ac.in (K. Sarkar).
[1]Authors are equally contributed

https://doi.org/10.1016/j.ijbiomac.2020.07.315
0141-8130/© 2020 Elsevier B.V. All rights reserved.

by Ghosh group [34] and Sinha Ray group [36] using chitosan and *Rubus fairholmianus* extract stabilised AgNPs, respectively. Hence, it was hypothesized that CD based AgNPs may be an efficient anticancer agent for cancer therapy.

Here, we report the synthesis of CD from natural polysaccharide presented in sweet lemon peel by simple hydrothermal process followed by in situ synthesis of AgNPs using CD acted as reducing as well as stabilizing agent at room temperature. Generally sweet lemon peel was recognised as a food waste. Here we used these waste lemon peel as a resource to develop CD and subsequently used these CD to synthesize AgNPs in situ. The synthesis of CD based AgNPs (CD@AgNPs) was characterized by UV–Vis spectroscopy, fluorescence spectrophotometer, XRD and TEM. The cytotoxicity of CD@AgNPs was optimized against MCF7, HeLa and OP9 (mouse bone marrow stromal cells) cells and the underlying mechanism for cytotoxicity was also observed.

2. Materials and methods

Fresh sweet lemon peels were collected from local juice shop in Kolkata, India. Silver nitrate ($AgNO_3$) and (3-(4,5-dimethylthiazol-2-yl)-2,5-diphenyltetrazolium bromide) (MTT) were purchased from SRL Pvt. Ltd. Dulbecco's modified eagle's media (DMEM), fetal bovine serum (FBS), penicillin–streptomycin, trypsin–EDTA, Dulbecco's phosphate buffered saline (DPBS), 2′,7′-dichlorofluorescin diacetate (DCFDA), TritonX-100 and molecular grade water were obtained from HiMedia Laboratories Private Limited, India. Paraformaldehyde and 4′,6-diamidino-2-phenylindole (DAPI) were purchased from Sigma-Aldrich. Sodium chloride (NaCl), tryptone, yeast extract and agar were brought from Merck, India. Phalloidin-iFluor 594 was purchased Abcam, USA. All other chemicals were analytical grade and used as received.

2.1. Synthesis of carbon dot (CD)

Carbon dot (CD) was prepared from sweet lemon peels using hydrothermal method according to our previous report [8] with slight modification. Briefly, fresh sweet lemon peels were collected from local juice shop and washed with double distilled water several times and chopped into small pieces and dried at 40 °C. Subsequently, 5 g of the dried peels were taken in a 100 ml hydrothermal chamber with 50 ml of water and the reactor was kept in an oven at 180 °C. After 3 h of reaction, the hydrothermal reactor was cooled down at room temperature and the brown coloured solution was decanted and subsequently filtered through 0.22 μm syringe filter followed by rotary evaporation (Model: Hei-VAP Advantage, Heidolph, Germany). Finally, the solution was lyophilised overnight to obtain the dry CD in powder form.

2.2. Synthesis of CD based silver nanoparticles (CD@AgNPs)

In situ CD@AgNPs was synthesized by a facile green method at room temperature (30 °C) without using any toxic chemicals. In brief, CD was dissolved in double distilled water taken in 10 ml glass vial. After getting CD solution, required amount of solid silver nitrate was added to the CD solution under constant stirring at room temperature. The synthesis of CD@AgNPs was optimized either by varying reaction time such as 5, 15, 30, 45, 60, 90, 120 and 180 min or by varying $AgNO_3$ concentrations such as 11, 17, 23, 28 and 34 mM or by varying CD concentrations such as 17, 34, 68, 102 and 137 μg/ml while keeping the other two parameters kept constant. The synthesis of CD@AgNPs was confirmed by UV–Vis spectrophotometer as AgNPs shows strong surface plasmon resonance (SPR) peak ~430 nm. The stability of CD@AgNPs was checked at room temperature by keeping it for more than one month.

2.3. Characterization

The UV–vis spectra of CD and CD@AgNPs were measured using Perkin Elmer Lambda 25 UV–vis spectrophotometer in between 200 and 800 nm using 1.0 cm path length quartz cuvette. Fluorescence spectra of CD and CD@AgNPs at different excitation and emission were performed by Horiba Fluoromax-3 spectrofluorometer using 1.0 cm path length quartz cuvette. The fluorescence lifetime was measured using a picosecond pulsed diode laser based TCSPC fluorescence spectrometer with $\lambda_{ex} = 340$ nm and MCP-PMT as a detector at room temperature. The emission from the samples was collected at right angle to the direction of the excitation beam maintaining magic angle polarization (54.7°) with a band pass of 2 nm. FTIR spectra of CD were recorded by Perkin Elmer Spectrum 100 FTIR at a frequency range of 4000–600 cm^{-1} with 48 consecutive scans at 1 cm^{-1} resolution. The morphology and particle size of CD and CD@AgNPs were characterized by TEM (JEM-2100F, JEOL, Japan) at 200 kV on a carbon coated copper grid. The XRD spectra of CD & CD@AgNPs were analysed by a wide angle X-ray scattering diffractometer (Panalytical X-ray diffractometer) with Cu Kα radiation (1.544 Å) within the range of 5–80 (2θ) at 40 kV and 30 mA.

2.4. Antimicrobial Activity of CD@AgNPs

The antimicrobial activity of CD@AgNPs was carried out by direct contact method according to the previous work [37]. Gram negative bacteria *Escherichia coli* (*E coli*) was cultured in Luria-Broth (LB) media for overnight at 37 °C with continuous shaking. After that, diluted bacteria suspension having optical density (OD) was added with CD@AgNPs solution with various concentrations (0.25, 0.5, 1.0, 1.5, 2.0 and 5.0 μg/ml). After incubating the above solution mixture at 37 °C for 2 h, the bacteria were isolated by centrifugation at 4 °C followed by washing with sterile PBS for three times. Finally, the bacteria were suspended in fresh LB media and consequently 200 μl of bacteria suspension was spread on LB agar plate followed by incubation at 37 °C for overnight. The images of agar plates were captured by BIOTOP gel doc system.

Separately, another part of the diluted treated bacteria suspension was cultured at 37 °C with constant shaking for overnight. The OD was measured at 578 nm and the percent of bacterial growth inhibition were calculated by following equation.

$$\%Inhibition = \frac{Abs_{control} - Abs_{test}}{Abs_{control}} \times 100$$

where, $Abs_{control}$ and Abs_{test} are the absorbance value of untreated and treated bacteria solution, respectively at 578 nm. Untreated bacteria were used as negative control whereas ampicillin was used as positive control. All tests were carried out in triplicate.

2.5. Cell culture

MCF-7 (human breast adenocarcinoma) and HeLa (Human Cervical Adenocarcinoma) cells were obtained from National Centre for Cell Sciences (NCCS) Pune, India. OP9 (Mouse embryonic stem cells) was purchased from ATCC, USA. These cells were cultured in DMEM medium with high Glucose containing 10% (v/v) fetal bovine serum (FBS, Gibco Life Technologies), 1% (v/v) penicillin–streptomycin (Sigma-Aldrich, USA) at 37 °C in a CO_2 incubator (Esco, Singapore) maintaining at 95% humidity and 5% CO_2.

2.6. In vitro cytotoxicity assay

MTT assay was employed to evaluate cytotoxicity of CD and CD@AgNPs on MCF-7, HeLa and OP9 cells. Briefly, cells were seeded in 96 well plate at a density of 5×10^3 cells per well and incubated in a CO_2 incubator for 24 h. After that, the media of each well was replaced with fresh media containing, different predetermined concentrations of CD and CD@AgNPs (5, 10, 25, 50, 100, 200 and 500 μg/ml) and incubated for a time period of 24 and 48 h. Thereafter, the media was discarded from each well and 100 μl of fresh DMEM media containing

10 μl MTT solution (5 mg/ml) was added in each well. After incubation at 37 °C for 4 h, purple coloured formazon crystals were dissolved by adding 100 μl of DMSO. Subsequently, the absorbance was measured at 570 nm by ELISA plate reader (Erna Lisa Scan EM, TRANSASIA, India). All experiments were performed in triplicate and represented by means of three measurements (±SD). The percent cells viability was calculated using the following equation.

$$\%Cell\ viability = \frac{Abs_{570\ (sample)}}{Abs_{570\ (control)}} \times 100$$

where, $OD_{570\ (sample)}$ and $OD_{570\ (control)}$ are the absorbance of sample and control, respectively at 570 nm.

2.7. Effect of CD@AgNPs on cell morphologys

Effect of CD@AgNPs on cell morphology was evaluated on MCF-7 cells at different concentrations of 10 and 50 μg/ml. Prior to the addition of CD@AgNPs, 1×10^5 cells were seeded in each well of 24 well plate containing sterilized cover slip. After reaching 70–80% confluency, cultured media was replaced with fresh media containing 10 and 50 μg/ml of CD@AgNPs and incubated at 37 °C in CO_2 incubator. Untreated cells were used as control. After 24 h of incubation, the cells were fixed with 4% paraformaldehyde solution after discarding the treated solution followed by washing with PBS thrice. After that 0.1% Triton X-100 was added and incubated for 3–5 min for cellular permeabilization. After washing with PBS for three times, 100 μl of 1× phalloidin working solution was added to each well and incubated at room temp for 90 min. Thereafter, 100 μl of DAPI solution was added after washing the cells with PBS thrice and again incubated in dark for 5 min followed by removing the staining solution carefully and washing with PBS for three times. Finally, coverslips were taken out from the wells and mounted on glass slides using glycerol as mounting media and consequently the images were captured by confocal laser scanning microscope (CLSM, Olympus FV3000). The area of the cells and the nuclei were measured using Image J software and plotted by Graphpad Prism software.

2.8. Intracellular reactive oxygen species (ROS) generation

After exposing with different concentration of CDs and CD@AgNPs, intracellular ROS generation were analysed qualitatively by Confocal Imaging where 2′,7′-dichlorodihydrofluorescein diacetate (DCFH-DA) was used as ROS detection probe. For this assay, Cells were seeded on coverslip in 24-well plate at density of 10^5 cells/well & grown for overnight, then cells were treated with desired concentrations of CDs and CD@AgNPs for 24 h. After 24 h 20 μM of DCFH-DA stain was added in each well and incubate for 20 min at 37 °C in dark. The positive controls were treated with 10 mM H_2O_2 for 2 h. Immediately after incubation, 4% paraformaldehyde was used to fix the cells for 15 min followed by washing with 1× PBS thrice. Then coverslips were mounted onto glass slides to evaluate under confocal microscopy.

2.9. Apoptosis assay

CD@AgNPs triggered apoptosis was evaluated by Alexa Flour 488 Annexin V/Dead cells apoptosis kit (ThermoFisher Scientific) using manufacturer protocol. Briefly, MCF 7 cells were cultured at a density of 10^5 cells/well of 24 well plate in presence of CD@AgNPs (50 μg/ml) for 24 h at 37 °C in CO_2 incubator. After that period, media was discarded and washed with cold PBS followed by centrifugation to discard the supernatant. Then cells were resuspended in 1× annexin binding buffer, 20 μl of annexin V conjugate and 1–2 μl of PI working solution (100 μg/ml) was added to each 100 μl of cells suspension. After 15 min of incubation at room temperature cells were washed with 1× annexin binding buffer followed by deposition of that suspension on glass slides to observe under confocal microscope.

3. Results and discussion

3.1. Structural characterization

Here we have developed a nano-conjugate comprising both CD and AgNPs (CD@AgNPs) to evaluate its efficacy for anticancer and antibacterial properties. For that we have synthesized CD from sweet lemon peel and AgNPs was prepared based on the reductive and stabilizing potency of thus prepared CD. The synthesis scheme was demonstrated in Fig. 1.

The optical properties and formation of CD and CD@AgNPs were analysed through different spectroscopic and microscopic studies. Fig. 2a depicts the presence of characteristic absorption spectrum of CD at 282 nm, which is due to the π-π* electronic transition of sp^2 hybridized C═C bonds which could justified by the previous report of Ghosh et al. and De et al. [8,20] indicating the formation of CD. However, after addition of silver nitrate into the CD solution, there is a generation of another new peak at 433–453 nm due to the formation of AgNPs (Fig. 2b, c and d).

It is previously reported that silver nanoparticles exhibit a strong absorbance band between 400 nm to 450 nm due to size dependent Surface Plasmon Resonance (SPR) properties [38,39]. Three parameters were varied during the CD mediated synthesis of silver nanoparticles i.e. time, concentration of silver nitrate and concentration of CD. Fig. 2b–d represents the effect of time, concentration of silver nitrate and CD, respectively on the formation of CD@AgNPs. From Fig. 2b we could observed that initially, in between the time span of 0 to 15 min of reaction no nanoparticles were formed, as at 433 nm no peak could be observed, after 15 min of reaction formation of AgNPs starts and continues upto 180 min. After 180 min, no significant change was observed in plasmon peak of the silver nanoparticles on UV–Vis spectra, which confirmed the complete formation of AgNPs. Fig. 2c depicts change in absorbance spectra with different concentrations of silver nitrate while taking fixed concentration of CD solution (137 μg/ml). We observed that the silver nanoparticles are forming in presence of all concentrations of silver nitrate starting from 11 mM to 34 mM. Although there is no significant change was observed in λ_{max} of silver nanoparticles, which suggests that, 137 μg/ml of CD solution have enough capability to reduce all the silver ions to silver nanoparticles. However, among all these concentrations silver nanoparticles made from of 11 mM and 17 mM silver nitrate concentrations than the others, with a stability of more than one month. The stability of the CD@AgNPs was measured in terms of UV Vis spectra study of the nanocomposite. Where no decrease in 433 nm AgNPs peak intensity was observed after 30 days of synthesis suggesting the nanocomposite is quite stable after one month. So, we choose CD@AgNPs made with 17 mM concentrations of silver nitrate for further studies. Fig. 2d shows, the UV–Vis absorbance spectra of CD@AgNPs composite with different concentrations of CD and fixed concentration of $AgNO_3$ addition i.e. 17 mM. From this figure, we found that CD are unable to reduce all silver ions to silver at low concentrations of CD (17, 34, 68 μg/ml). Silver nanoparticles formed better at higher concentrations of CD i.e. 102 and 137 μg/ml of CD. Finally, we used 137 μg/ml of CDs for synthesizing CD@AgNPs at room temperature after 3 h of reaction. The in situ formation mechanism of AgNPs in presence of CD, due to presence of hydroxyl (–OH) and (–COOH) groups in CD surface, which takes part to reduce the silver(I) (Ag^+) ions to silver (0) (Ag^0) nanoparticles. The presence of –OH and –COOH groups in CD surface were confirmed by FTIR spectroscopy which was demonstrated in Fig. S1. The broad peak at 3308 cm^{-1} was due to the stretching vibration mode of –OH group [40]. Peak at range of 1590 cm^{-1} to 1400 cm^{-1} was due to asymmetric and symmetric stretching of $–COO^-$ group [28]. Due to –C-OH stretching another peak was observed at 1275 cm^{-1}. Another characteristic peaks were present at 2930 cm^{-1} and 812 cm^{-1} indicated the presence of –C—H stretching and –C—H out of plane bending respectively. Peak at 1765 cm^{-1} was present due to carboxylic acid –C═O stretch. Additionally, at 1660 cm^{-1}, a peak was detected due to aromatic C═C bending.

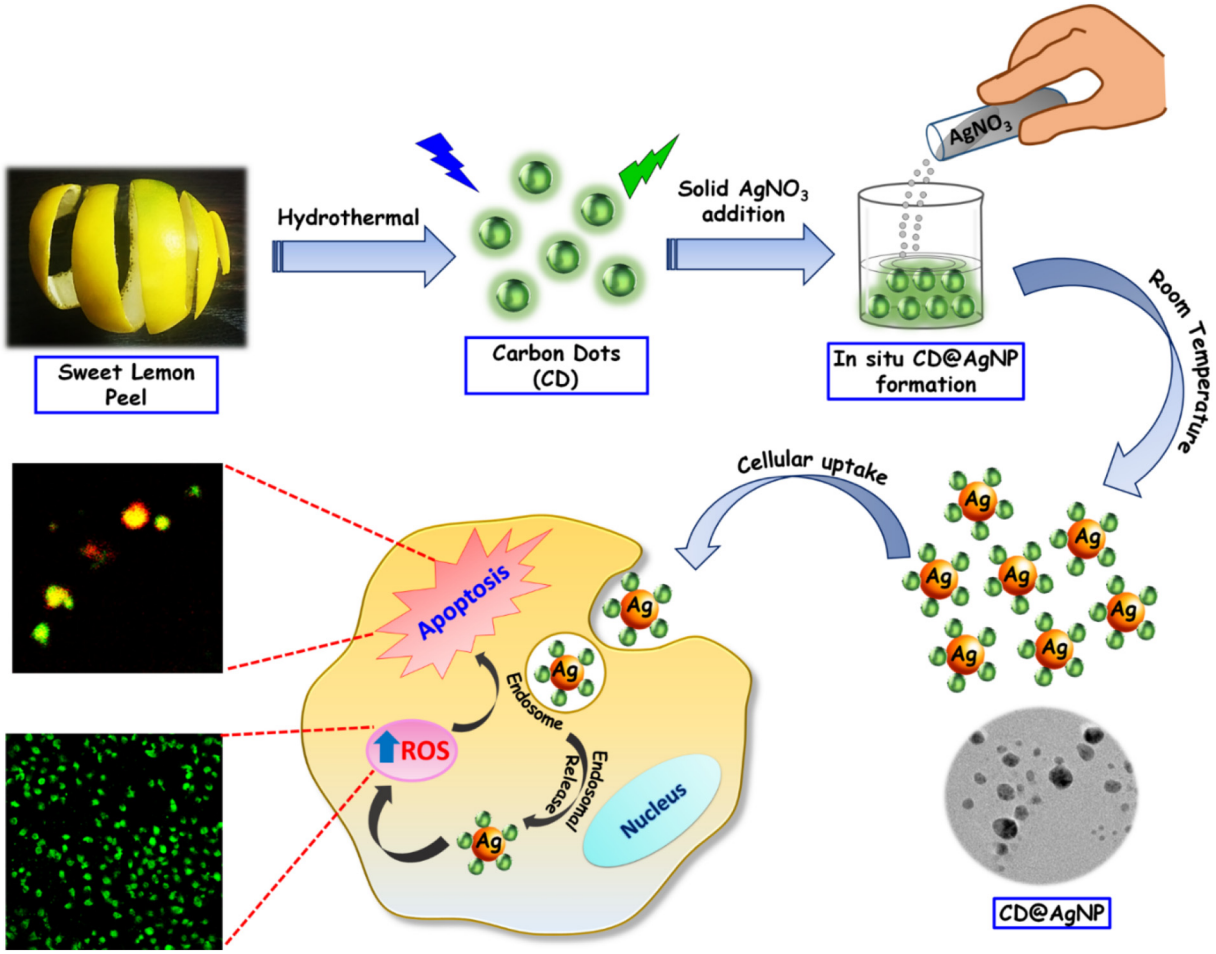

Fig. 1. Schematic representation of CD@AgNPs synthesis with their probable cellular activity toward breast cancer cells.

Fig. S2 demonstrated the XRD spectra of as synthesized CD and CD@AgNPs nanocomposite. It is well established that CD shows a broad spectrum due to its amorphous nature. However, due to presence of graphitic like structures of in its core it showed a broad hump around 23.8° with a plane of (002) and interlayer spacing of 4 Å which is slightly greater than pure bulk graphite. Pure graphite demonstrates d spacing of 3.3 Å [41,42]. After formation of CD@AgNPs, presence of two sharp peak could be observed due to highly crystalline nature of AgNPs along with a broad hump of CD. The two sharp peak at 38.8° and 65° in CD@AgNPs corresponding to the (111) and (200) plane of AgNPs with a lattice spacing of 2.315 Å and 1.433 Å confirms the presence of AgNPs into the composite which is similar to previous reported data [43,44].

To further explore the optical properties of the synthesized CD and CD@AgNPs, we have tested the fluorescence properties of both the material. Fig. 3a demonstrates a typical green fluorescence of CD upon irradiation of UV (365 nm) light. Upon different fluorescence excitation CD demonstrated excitation dependent emission behaviour as the emission maxima of CD shifts as excitation wavelength changes. The maximum fluorescence emission intensity of CD was observed at 432 nm upon excitation wavelength with 360 nm (Fig. 3b). This excitation dependent behaviour of CD indicates the presence of multiple distinct emission sites on the CDs. Based on the previous studies it can be said that, these multiple emission sites are correlated with the sp^2 sub-regions which are present in carbon core (supported by XRD data Fig. S2), as well as due to the several functional groups on the surface of the CD [45,46]. While the fluorescence intensity quenched after addition of silver nitrate. This may be due to the photo-induced electron transfer between CD and forming silver nanoparticles [47]. On the other hand, fluorescence life time decay curves and average life time of CDs were calculated. From Fig. 3d, it can be said that the half-life of CDs is 6.9 ns.

The morphology and size distribution of CDs and CD@AgNPs were investigated with the help of transmission electron microscopy (TEM). From Fig. 4a it could be observed that the synthesized CDs were well dispersed having a size distribution from 2 to 6 nm. When CD@AgNPs were synthesized from CD they found to have well dispersed with a size in between 5 and 16 nm (Fig. 4b). Further high resolution images confirmed that the CD@AgNPs were highly crystalline in nature (Fig. 4c). The lattice fringes of AgNPs can be observed in Fig. 4c with a distance between two lattice planes of 1.43 Å which supports the XRD data of AgNPs with a lattice plane of (111). Fig. 4d also exhibit well dispersed CD and AgNPs in the nanocomposite.

3.2. Antibacterial study of CD@AgNPs

It is crucial to check antimicrobial activity of any biomaterial prior to their use, to avoid any undesirable infections during their applications. If a biomaterial does not possess any antimicrobial activity special care should be taken during its storage and application. In this context silver nanoparticles are well known for its superior antimicrobial activity. In this work we also evaluated the antibacterial efficacy of CD@AgNPs. For this study *E. coli*, a gram negative strain bacteria were chosen. Ampicillin was used as a reference standard. Fig. S3a depicted the percent inhibition of *E. coli* in presence of different concentrations of CD@AgNPs. It showed that significant inhibition was started at a concentration of 1.5 μg/ml and it achieved 80% at 5.0 μg/ml. Pal et al. have shown that 50 to 100 μg of spherical silver nanoparticles can cause almost 100% inhibition of bacterial growth which indicate the superior antibacterial

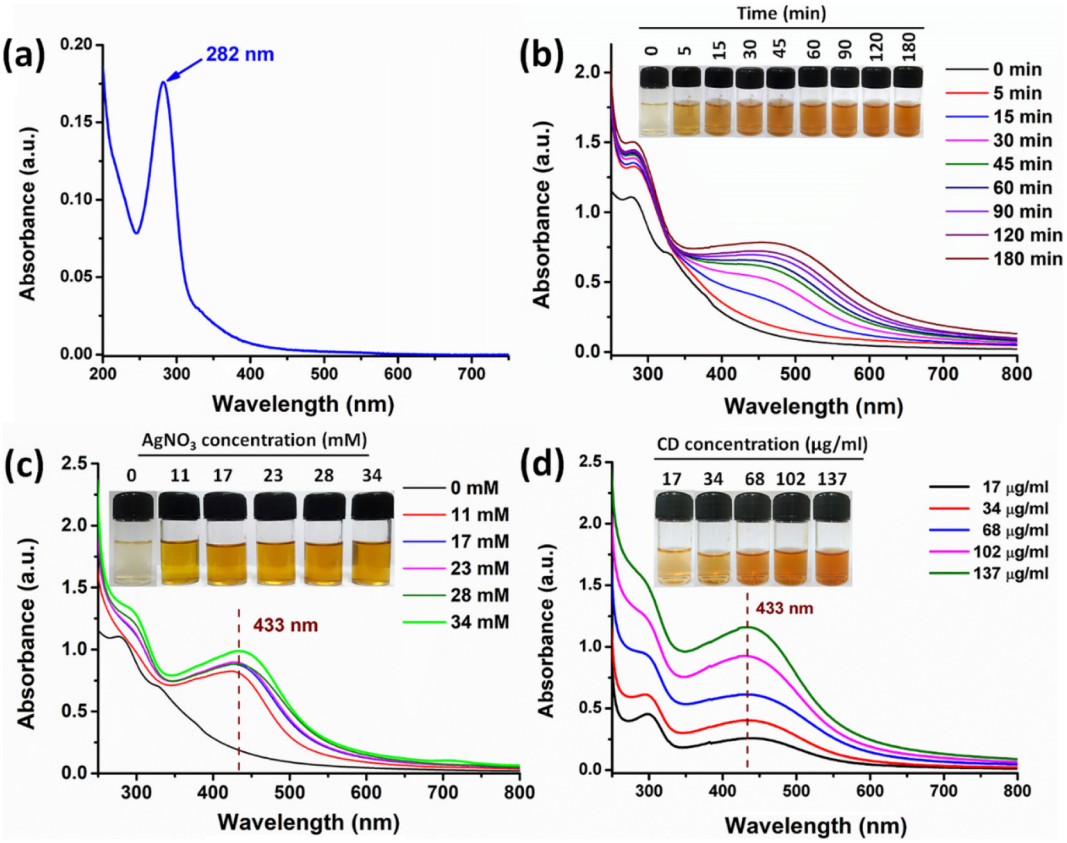

Fig. 2. UV–vis spectra of CD (a); effect of time during the synthesis of CD@AgNPs (b); effect of silver nitrate concentration during the synthesis of CD@AgNPs (c) and effect of CD concentration during the synthesis of CD@AgNPs (d).

potency of CD@AgNPs than other previously synthesized silver nanoparticles [48]. We also checked the antibacterial efficacy of bare CD however it did not demonstrate any antimicrobial response as high as 500 μg/ml concentration (data not shown). So it can be confirmed that, the antibacterial response of CD@AgNPs actually come from AgNPs which are present in CD@AgNPs nanocomposite. When bacterial growth on agar plate was evaluated in presence of 1.5 and 5.0 μg/ml of CD@AgNPs (Fig. S3b), initial inhibition of bacterial growth was observed at 1.5 μg/ml and almost no bacterial growth could be observed on the plate containing 5.0 μg/ml of CD@AgNPs, which in turn indicated the superior bactericidal efficacy of CD@AgNPs.

Cytotoxicity study

MTT assay was performed to evaluate in vitro cytotoxicity of CD and CD@AgNPs against MCF 7, Hela and OP9 cell line. Those cell lines were exposed to different concentrations of CD and CD@AgNPs (5, 10, 25, 50, 100, 200 and 500 μg/ml) for 24 h and 48 h.

Cytotoxicity and biocompatibility of CD sometime differ with their source. Like according to Arkan et al. the IC_{50} value of Walnut Oil derived CD was found to be 1.25 ± 0.062 μg/ml after 24 h of incubation against MCF 7 [49]. Whether, CD derived from sugarcane molasses by Huang et al. remain non-toxic at even 4 mg/ml concentration against the same cell line [50]. The reason behind it still not known. When we evaluate the IC_{50} value of our CD, it was found to be 10 μg/ml for MCF 7 after 24 h whether after 48 h it was 500 μg/ml (Fig. 5a, b). Which indicated that initial 24 h the CD might have shown toxicity at low concentration but with time it remains non-toxic till 200 μg/ml. However, in case of Hela cell line we have found that CD have the IC_{50} value ˂ 500 μg/ml after 24 h which increases to 500 μg/ml after 48 h (Fig. 5c, d). So, CD remain non-toxic at 200 μg/ml in case of Hela cell line also. When the effect of CD was observed on Embryonic Stem Cells (OP9), it was found to be non-toxic at even higher concentration for 24 h as well as 48 h (Fig. 5e, f). CD derived CD@AgNPs have shown superior cytotoxicity over MCF 7 and HeLa than the CD itself. After 24 h of incubation, IC_{50} value of CD@AgNPs was found to be ˂ 10 μg/ml in case of MCF 7 cell line (Fig. 5a). As the concentration of CD@AgNPs increased, the anticancer efficacy was increased as well, the result remains almost same after 48 h. Our CD@AgNPs have shown greater potency than previously derived silver nanoparticles by Bhanumathi et al. showed the IC_{50} value of almost 40 μg/ml against MCF 7 cell line [51]. However, against HeLa cell line, the IC_{50} value of CD@AgNPs was found to be 10 μg/ml and remained same till 25 μg/ml (Fig. 5c). The IC_{50} value as well as the effect of concentration of CD@AgNPs over MCF 7 and HeLa cell line depicted that CD@AgNPs was most effective against the breast cancer cell line MCF 7. The result could be justified by the previous findings like Salazar et al. was synthesized silver nanoparticles from *G. neuberthii fruit* and *P. americana* leaf [52] and evaluate their cytotoxicity over MCF-7 and HeLa. They have found that silver nanoparticles were more effective against MCF 7 than HeLa. According to Salazar et al. it might be due to the reduced cellular uptake of silver nanoparticles by HeLa compared to the MCF-7 cell line [52]. The effect of CD@AgNPs on MCF 7 might be the synergistic effect of the CD too as compared to the cytotoxicity of CD on HeLa at 24 h. Fig. 5e and f depicted the cell viability of CD@AgNPs at 24 h and 48 h, respectively and found that it remained almost non-toxic at 100 μg/ml.

3.3. Cell morphology

Silver nanoparticles treatment can cause toxicity through morphological changes in different cancer cell line like human lung cancer and ovarian [53,54]. To determine whether CD@AgNPs could influence the cell morphology we evaluated MCF 7 cells treated with different concentrations of CD@AgNPs (10 and 50 μg/ml).

Fig. 6a–c showed untreated MCF 7 cells morphology. Nuclei of control cells was stained with DAPI (Fig. 6a), showed almost circular in

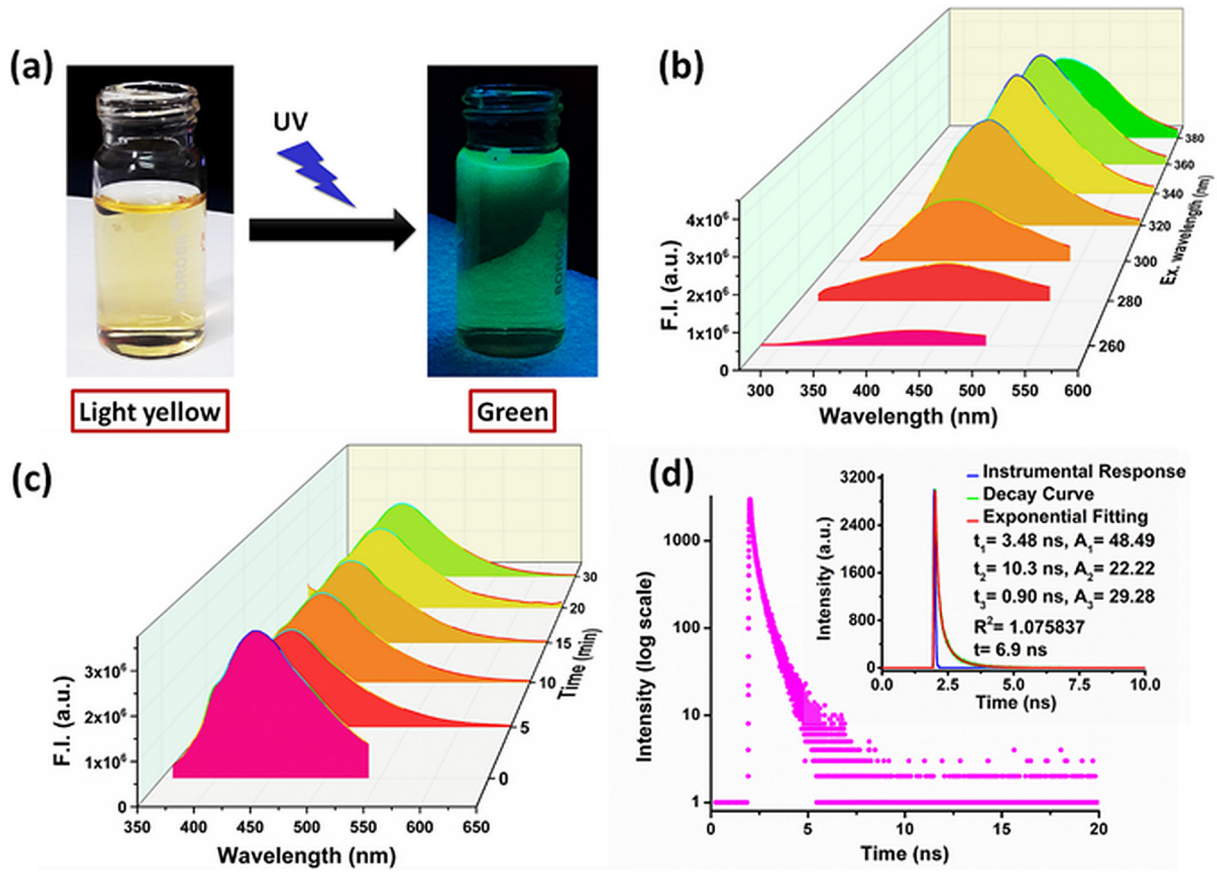

Fig. 3. Emission of green fluorescence upon irradiation of UV light on the CD solution (a); emission curve of CD upon excitation with different wavelength (b); quenching of fluorescence upon addition of $AgNO_3$ with excitation wavelength of 360 nm (c) and lifetime curve of CDs with 3rd order fitting (inset) (d).

shape and having the average area of 300 μM^2 (Fig. 6k). Phalloidin was used to stain the actin filaments indicating the whole cell periphery (Fig. 6b). Fig. 6b showed the normal cytoskeletal morphology of MCF 7 with the average area of 1806 μM^2 (Fig. 6j). Fig. 6c showed the merged image of untreated MCF 7, indicated the healthy cells cytoskeleton having define nuclei inside. When the MCF 7 cells were treated with 10 μg/ml of CD@AgNPs, where almost 60% inhibition happened in MTT assay, interestingly the morphology of the whole cell was not effected as such. Fig. 6d depicted that nuclei of the cells after treatment with 10 μg/ml of CD@AgNPs, showed circular nuclei with the average size area of 280 μM^2 (Fig. 6k). The cytoskeleton after the same treatment (Fig. 6e) was look similar as control having the average area of 2068 μM^2 (Fig. 6j). Merge image (Fig. 6f) showed control like morphology after the treatment of CD@AgNPs (10 μg/ml). However, 50 μg/ml of CD@AgNPs showed detrimental effect on cells morphology which could be easily visualized by the confocal microscopic image (Fig. 6g–i). Fig. 6g showed circular but significantly small in size nuclei like they were fragmented. The average area was significantly decreased to almost 100 μM [2] compared to the control or even the CD@AgNPs (10 μg/ml) treated one. After the treatment with 50 μg/ml of CD@AgNPs the shape of the cytoskeleton markedly changed, they were round in shape and few cases they were fragmented as well (Fig. 6h). When the cytoskeleton area of the CD@AgNPs (50 μg/ml) treated MCF 7 cells were compared with the control and CD@AgNPs (10 μg/ml) treated one, significant decrease could be observed and found to be 488 μM [2] (Fig. 6j). So, it could be established from this study that CD@AgNPs at a concentration of 50 μg/ml could initiate the morphological changes in MCF 7 cell line where shrinkage of cells as well as efflux of the cytoplasmic content could be observed. According to the Suzuki-Karasaki cell-shrinkage might be the indication of apoptosis which could be the results of the imbalance of Na^+, K^+ and other intracellular ion homeostasis [55].

3.4. Intracellular ROS generation

According to the previous reports, silver nanoparticles could trigger the generation of intracellular ROS leading to apoptosis of different cancer cells [56,57]. To evaluate the fact different concentration of CD and CD@AgNPs were studied for intracellular ROS generation. With respect of the cytotoxicity study the concentrations for this experiment was chosen. In this study DCFH-DA was used to detect the ROS generation. DCFH-DA itself is a non-fluorescent dye, when it internalized by the cells followed by enzymatic hydrolysis, it could produce DCFH. This DCFH could produce strong fluorescence after being oxidized by intracellular ROS [58]. So, strong fluorescence indicated the presence of more amount of ROS inside the cells. Fig. 7 shows the effect of concentration in the generation of intracellular ROS. From Fig. 7a–c, it could be found that in the concentration of 50, 200 and 500 μg/ml of CD could trigger the production of intracellular ROS. It could be also observed that the fluorescence intensity was increased with increasing concentration of CD, which indicated the concentration dependent ROS generation leading to cell death. It could also be justified by the cytotoxicity data of CD against MCF 7 (Fig. 5a). When similar concentrations CD@AgNPs were used to evaluate the ROS generation capability, superior result was found than CD. Increased fluorescence intensity could be observed at concentration of 200 μg/ml (Fig. 7e) than 50 μg/ml (Fig. 7d), which could be explained by the increased generation of ROS in case of 200 μg/ml of CD@AgNPs. However, at the concentration of 500 μg/ml interestingly almost no fluorescence could be observed. This phenomenon could be justified by the fact that, in presence of

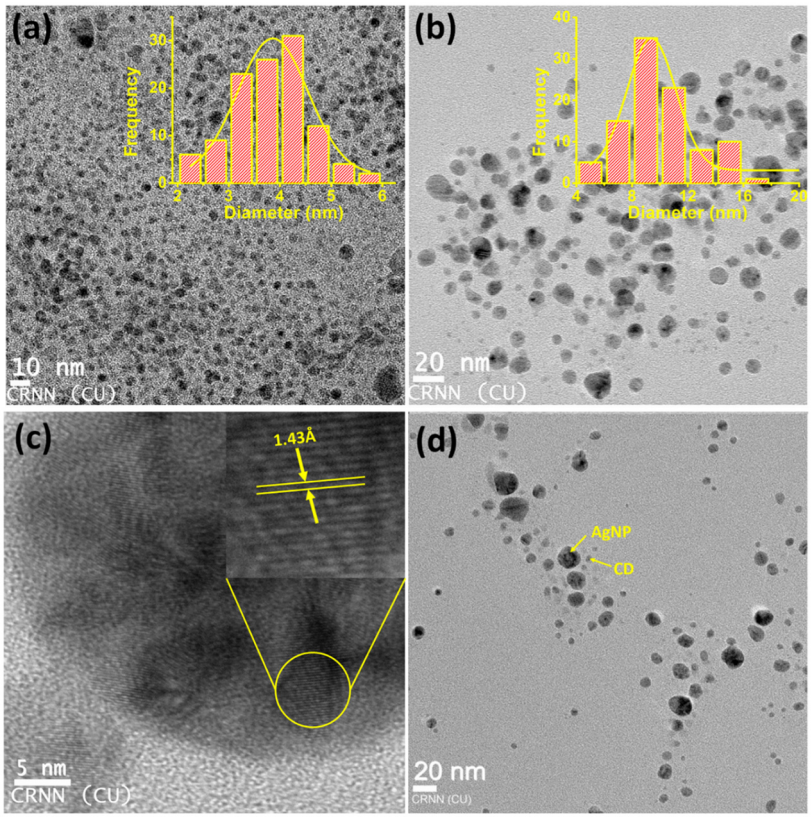

Fig. 4. TEM image of CD and corresponding size distribution curve (a); TEM image of CD@AgNPs and corresponding size distribution curve of AgNPs (b); ultra-magnified image showing lattice fringe of AgNPs (c) and TEM image with distinguishable both AgNPs and CDs (d).

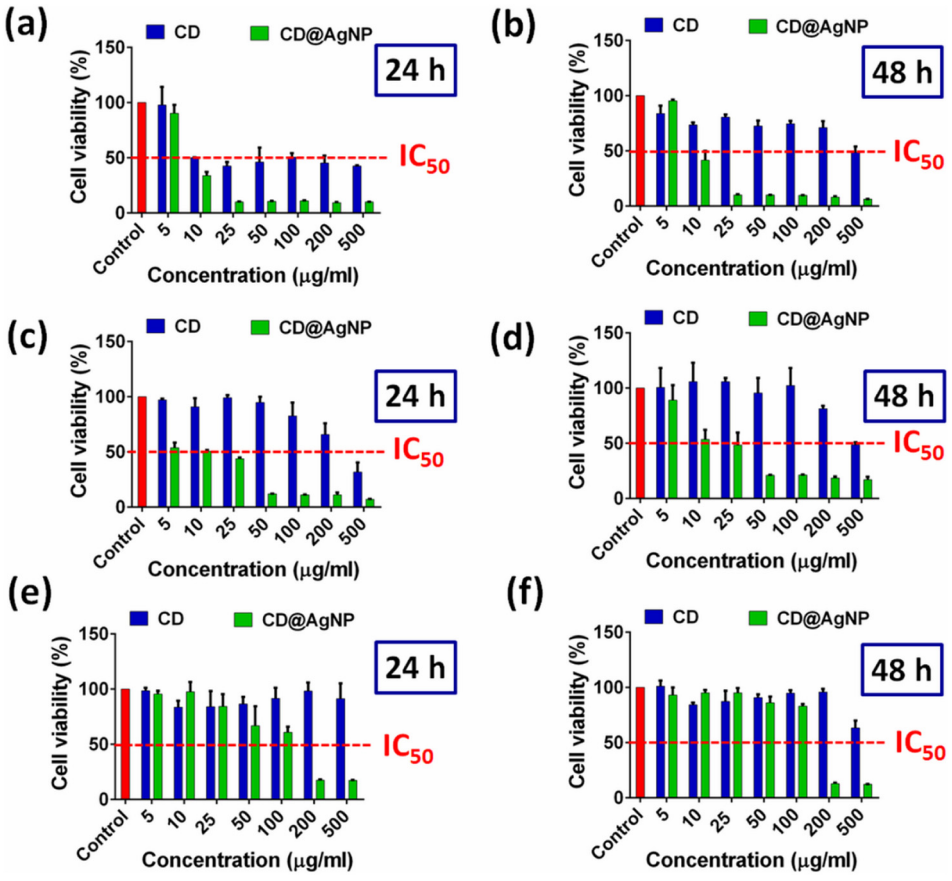

Fig. 5. Cytotoxicity assay of CD and CD@AgNPs against MCF 7 breast cancer cells (a, b), Hela (c, d) and mouse embryonic OP9 cell line (e, f).

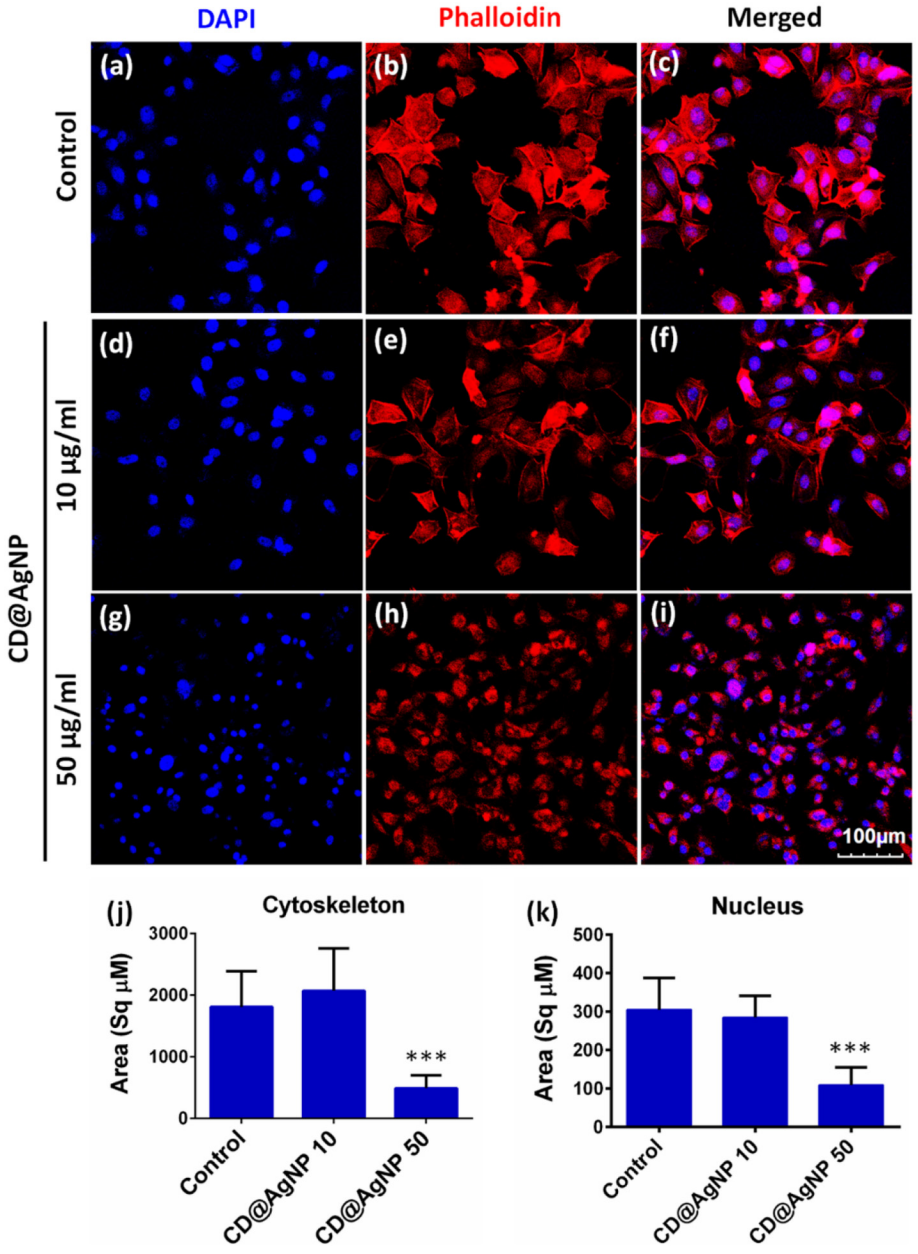

Fig. 6. Effect of CD@AgNPs on the cell morphology of MCF-7 after 24 h of treatment. Nuclei stained with DAPI (without treatment) (a); image of cytoskeletons stained with Phalloidin (without treatment) (b); merged image of DAPI and Phalloidin (without treatment) (c); nuclei stained with DAPI after treating with 10 µg/ml of CD@AgNPs (d); image of cytoskeletons stained with Phalloidin after treating with 10 µg/ml of CD@AgNPs) (e); merged image of DAPI and Phalloidin after treating with 10 µg/ml of CD@AgNPs) (f); nuclei stained with DAPI after treating with 50 µg/ml of CD@AgNPs (g); image of cytoskeletons stained with Phalloidin after treating with 50 µg/ml of CD@AgNPs) (h); merged image of DAPI and Phalloidin after treating with 50 µg/ml of CD@AgNPs) (i) calculated cytoskeletons and nuclei area after treatment with different concentrations of CD@AgNPs (j, k).

500 µg/ml of CD@AgNPs, no cell was survived to response in DCFH-DA assay. This fact indicated that CD@AgNPs could trigger the production intracellular ROS, which in turn increase the oxidative stress leading to apoptosis. Cytotoxicity data of CD@AgNPs (Fig. 5a) and effect of CD@AgNPs on cell morphology (Fig. 6) could be justified by this result.

3.5. Apoptosis study

Apoptosis plays an important role in cell homeostasis and their morphological and biochemical changes [59]. Silver nanoparticles mediated apoptosis in cancer even in bacterial cells are well established according to the several previous reports. To evaluate the apoptotic potential of CD@AgNPs, we have carried out a qualitative apoptosis assay using confocal microscopy. Annexin V/PI staining revealed the apoptotic and non-apoptotic cells.

The results of staining (Fig. 8) displayed green fluorescence due to the annexin V conjugate (Fig. 8a, a′), red fluorescence for PI (Fig. 8b, b′), fluorescence merged field (Fig. 8c, c′) and merged image in bright field (Fig. 8d, d′). The basic concept behind this staining based apoptosis assay was that through calcium dependent binding annexin V could bind to phosphatidylserine (PS), flipped outside of the cell membrane during early stage of apoptosis whether PI could bind to the nucleic acid whenever cell lost its integrity because PI couldn't penetrate through the healthy cell membrane indicated the late apoptosis. To evaluate the findings, we manually zoomed out a selected portion of the image (Fig. 8b′) which showed that cells with green fluorescence as well as green and red fluorescence, which in turn indicated that the different stages of CD@AgNPs mediated apoptosis i.e. early apoptosis (EAp) (Annexin V+/PI−) and late apoptosis (Lap) (Annexin V+/PI+). Necrotic/dead cells could also be found showed only red

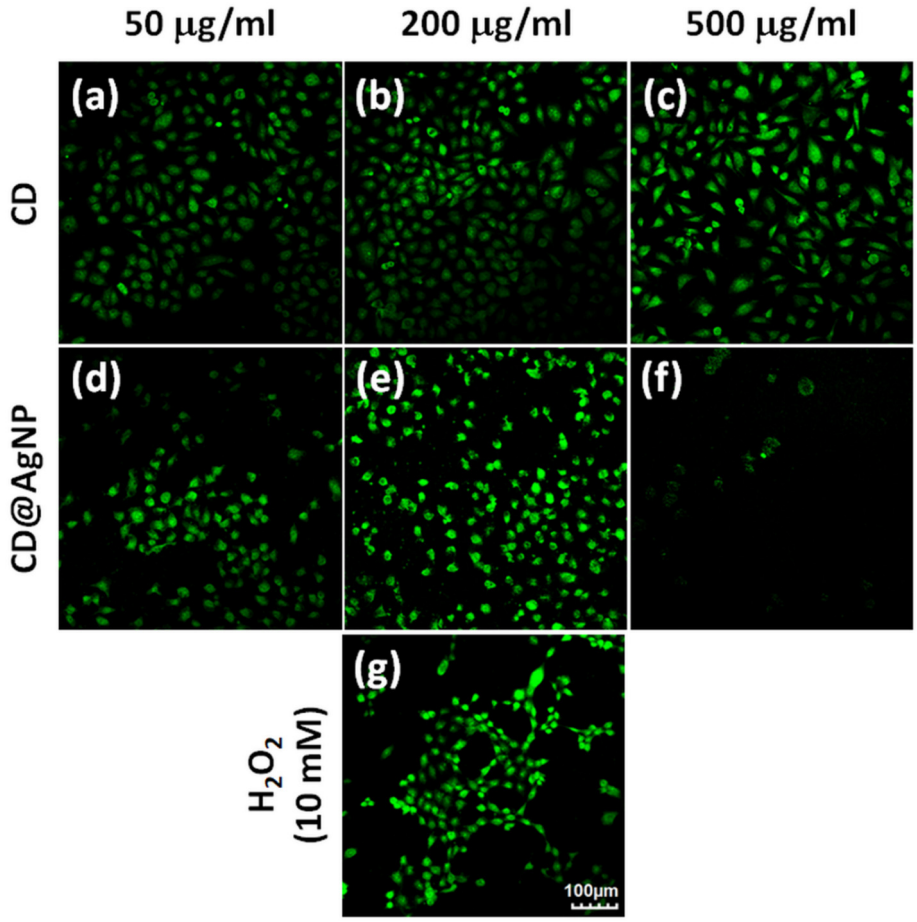

Fig. 7. Generation of intracellular ROS was evaluated in presence of CD, CD@AgNPs and H_2O_2 in MCF-7 breast cancer cells. MCF-7 breast cancer cells treated with 50 μg/ml CD (a); 200 μg/ml CD (b); 500 μg/ml CD (c); MCF-7 cells breast cancer treated with 50 μg/ml CD@AgNPs (d); 200 μg/ml CD@AgNPs (e); 500 μg/ml CD@AgNPs (f); MCF-7 cells breast cancer treated with 10 mM H_2O_2 (g).

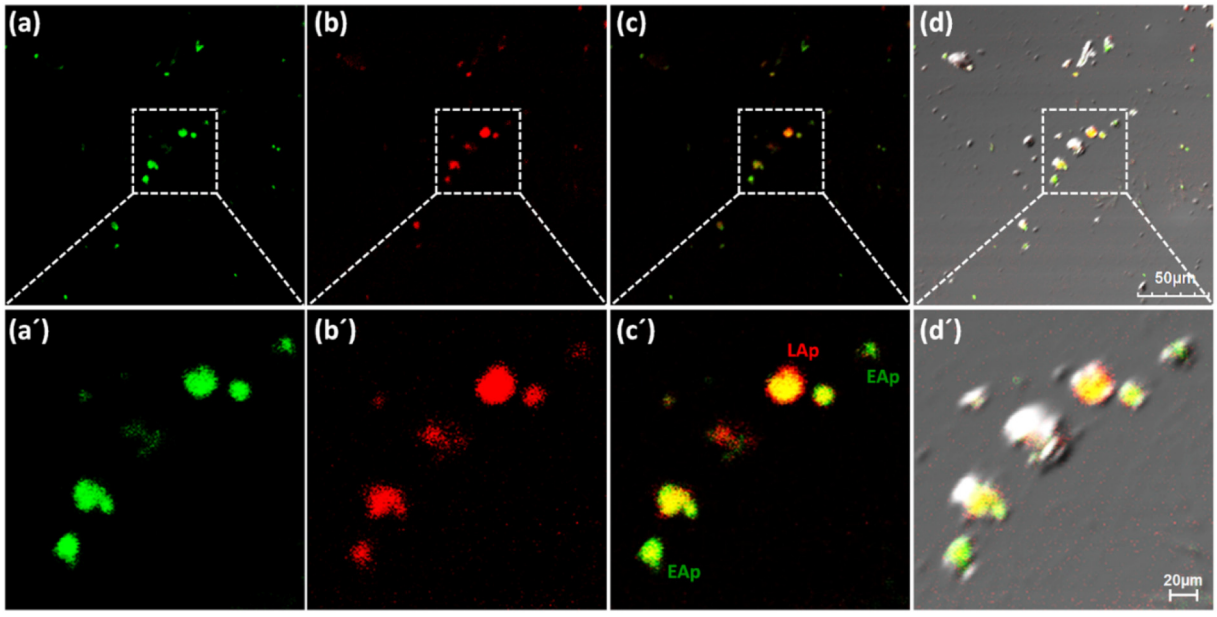

Fig. 8. Apoptosis assay in presence of CD@AgNPs (50 μg/ml) against MCF 7 cell line: green fluorescence due to the annexin V conjugate (a, a′), red fluorescence for PI (b, b′), fluorescence merged field (c, c′) and merged image in bright field (d, d′).

fluorescence (Annexin V−/PI+). This phenomenon of CD@AgNPs mediated apoptosis could be justified by our previous data, where we found significant changes of cellular morphology in presence of CD@AgNPs. It could be also noted that CD@AgNPs could trigger the intracellular ROS generation (Fig. 7d, e and f) leading to apoptosis. Similar result was also found by George et al. [36] when they studied the apoptosis potential of multifaceted biosynthesized silver nanoparticles on MCF 7 cells. They found that generation of intracellular ROS could damage the DNA leads to apoptosis. They have also found increased caspase 3/7 activity, release of cytochrome *c* and depolarization of mitochondrial membrane could be the mechanism behind the silver nanoparticles induced apoptosis.

4. Conclusions

We demonstrated the facile green synthesis of CD@AgNPs using CD synthesized from renewable resource. Here, CD performed as a reducing and stabilizing agent for the successful fabrication of CD@AgNPs in room temperature. CD@AgNPs showed excellent antibacterial potency against *E. coli* where almost 80% bacterial inhibition could be observed at a concentration of 5.0 μg/ml. The synthesized CD@AgNPs showed superior anticancer potency against MCF 7 breast cancer cells in a dose dependent manner. It could be observed that the anticancer activity of CD@AgNPs against MCF 7 is strongly related with the generation of intracellular ROS leading to apoptosis. Moreover, the synthesized CD possess some outstanding optical properties such as excitation dependent multicolor fluorescence emission, photo-stability etc. which could make them a bio imaging probe useful for the detection of any disease condition in future.

Declaration of competing interest

All authors declare no conflict of interest.

CRediT authorship contribution statement

Krishanu Ghosal: Data curation, Formal analysis, Writing - original draft, Software. **Santanu Ghosh:** Formal analysis, Writing - original draft, Software. **Debjani Ghosh:** Formal analysis, Software. **Kishor Sarkar:** Conceptualization, Data curation, Funding acquisition, Investigation, Methodology, Project administration, Resources, Software, Supervision, Validation, Visualization, Writing - review & editing.

Acknowledgement

KS acknowledge to DST-SERB for supporting financially through two sanctioned projects EEQ/2016/000712 and ECR/2016/002018. K.S. also acknowledge UGC for UGC-BSR Research Start-Up Grant (F.30-363/2017 (BSR), Dt-08/08/2017) and CU for UPE-II Nanofabrication project fund (UGC/166/UPE-II, Dt-03/04/2017) for financial support.

Appendix A. Supplementary data

Supplementary data to this article can be found online at https://doi.org/10.1016/j.ijbiomac.2020.07.315.

References

[1] S. Aftab, A. Shah, A. Nadhman, S. Kurbanoglu, S. Aysıl Ozkan, D.D. Dionysiou, S.S. Shukla, T.M. Aminabhavi, Nanomedicine: an effective tool in cancer therapy, Int. J. Pharm. 540 (1) (2018) 132–149, https://doi.org/10.1016/j.ijpharm.2018.02.007.

[2] A. Wicki, D. Witzigmann, V. Balasubramanian, J. Huwyler, Nanomedicine in cancer therapy: challenges, opportunities, and clinical applications, J. Control. Release 200 (2015) 138–157, https://doi.org/10.1016/j.jconrel.2014.12.030.

[3] Y. Matsumura, H.A. Maeda, New concept for macromolecular therapeutics in cancer chemotherapy: mechanism of tumoritropic accumulation of proteins and the antitumor agent Smancs, Cancer Res. 46 (12 Part 1) (1986) 6387–6392.

[4] L.E. Gerlowski, R.K. Jain, Microvascular permeability of normal and neoplastic tissues, Microvasc. Res. 31 (3) (1986) 288–305.

[5] M. Overchuk, G. Zheng, Overcoming obstacles in the tumor microenvironment: recent advancements in nanoparticle delivery for cancer theranostics, Biomaterials 156 (2018) 217–237.

[6] S. Tran, P.-J. DeGiovanni, B. Piel, P. Rai, Cancer nanomedicine: a review of recent success in drug delivery, Clin. Transl. Med. 6 (1) (2017) 44, https://doi.org/10.1186/s40169-017-0175-0.

[7] K. Ghosal, K. Sarkar, Biomedical applications of graphene nanomaterials and beyond, ACS Biomater. Sci. Eng. 4 (8) (2018) 2653–2703.

[8] S. Ghosh, K. Ghosal, S.A. Mohammad, K. Sarkar, Dendrimer functionalized carbon quantum dot for selective detection of breast cancer and gene therapy, Chem. Eng. J. 373 (2019) 468–484, https://doi.org/10.1016/j.cej.2019.05.023.

[9] S. Anwar, H. Ding, M. Xu, X. Hu, Z. Li, J. Wang, L. Liu, L. Jiang, D. Wang, C. Dong, M. Yan, Q. Wang, H. Bi, Recent advances in synthesis, optical properties, and biomedical applications of carbon dots, ACS Appl. Bio Mater. 2 (6) (2019) 2317–2338, https://doi.org/10.1021/acsabm.9b00112.

[10] K. Ghosal, A. Ghosh, Carbon dots: the next generation platform for biomedical applications, Mater. Sci. Eng. C 96 (2019) 887–903, https://doi.org/10.1016/j.msec.2018.11.060.

[11] Y.-P. Sun, B. Zhou, Y. Lin, W. Wang, K.S. Fernando, P. Pathak, M.J. Meziani, B.A. Harruff, X. Wang, H. Wang, Quantum-sized carbon dots for bright and colorful photoluminescence, J. Am. Chem. Soc. 128 (24) (2006) 7756–7757.

[12] H. Ming, Z. Ma, Y. Liu, K. Pan, H. Yu, F. Wang, Z. Kang, Large scale electrochemical synthesis of high quality carbon nanodots and their photocatalytic property, Dalton Trans. 41 (31) (2012) 9526–9531.

[13] K.K. Chan, C. Yang, Y.-H. Chien, N. Panwar, K.-T. Yong, A facile synthesis of label-free carbon dots with unique selectivity-tunable characteristics for ferric ion detection and cellular imaging applications, New J. Chem. 43 (12) (2019) 4734–4744, https://doi.org/10.1039/C8NJ06306K.

[14] T. Pal, S. Mohiyuddin, G. Packirisamy, Facile and green synthesis of multicolor fluorescence carbon dots from curcumin: in vitro and in vivo bioimaging and other applications, ACS Omega 3 (1) (2018) 831–843.

[15] Y. Wang, X. Chang, N. Jing, Y. Zhang, Hydrothermal synthesis of carbon quantum dots as fluorescent probes for the sensitive and rapid detection of picric acid, Anal. Methods 10 (23) (2018) 2775–2784, https://doi.org/10.1039/C8AY00441B.

[16] S. Zhao, M. Lan, X. Zhu, H. Xue, T.-W. Ng, X. Meng, C.-S. Lee, P. Wang, W. Zhang, Green synthesis of bifunctional fluorescent carbon dots from garlic for cellular imaging and free radical scavenging, ACS Appl. Mater. Interfaces 7 (31) (2015) 17054–17060.

[17] P. Mondal, K. Ghosal, S.K. Bhattacharyya, M. Das, A. Bera, D. Ganguly, P. Kumar, J. Dwivedi, R. Gupta, A.A. Martí, Formation of a gold–carbon dot nanocomposite with superior catalytic ability for the reduction of aromatic nitro groups in water, RSC Adv. 4 (49) (2014) 25863–25866.

[18] V. Ramanan, S.K. Thiyagarajan, K. Raji, R. Suresh, R. Sekar, P. Ramamurthy, Outright green synthesis of fluorescent carbon dots from eutrophic algal blooms for in vitro imaging, ACS Sustain. Chem. Eng. 4 (9) (2016) 4724–4731.

[19] J. Zhou, Z. Sheng, H. Han, M. Zou, C. Li, Facile synthesis of fluorescent carbon dots using watermelon peel as a carbon source, Mater. Lett. 66 (1) (2012) 222–224.

[20] B. De, N. Karak, A green and facile approach for the synthesis of water soluble fluorescent carbon dots from banana juice, RSC Adv. 3 (22) (2013) 8286–8290, https://doi.org/10.1039/C3RA00088E.

[21] S. Sahu, B. Behera, T.K. Maiti, S. Mohapatra, Simple one-step synthesis of highly luminescent carbon dots from orange juice: application as excellent bio-imaging agents, Chem. Commun. 48 (70) (2012) 8835–8837, https://doi.org/10.1039/C2CC33796G.

[22] N. Wang, Y. Wang, T. Guo, T. Yang, M. Chen, J. Wang, Green preparation of carbon dots with papaya as carbon source for effective fluorescent sensing of iron (III) and Escherichia coli, Biosens. Bioelectron. 85 (2016) 68–75.

[23] A. Kumar, A.R. Chowdhuri, D. Laha, T.K. Mahto, P. Karmakar, S.K. Sahu, Green synthesis of carbon dots from Ocimum sanctum for effective fluorescent sensing of Pb^{2+} ions and live cell imaging, Sensors Actuators B Chem. 242 (2017) 679–686.

[24] J. Shen, S. Shang, X. Chen, D. Wang, Y. Cai, Facile synthesis of fluorescence carbon dots from sweet potato for Fe^{3+} sensing and cell imaging, Mater. Sci. Eng. C 76 (2017) 856–864.

[25] I. Rahmawati, R. Intan, M. Zakaria, Photoluminescence study of carbon dots from ginger and galangal herbs using microwave technique, J. Phys. Conf. Ser. (2018) 012004 IOP Publishing.

[26] R. Bandi, B.R. Gangapuram, R. Dadigala, R. Eslavath, S.S. Singh, V. Guttena, Facile and green synthesis of fluorescent carbon dots from onion waste and their potential applications as sensor and multicolour imaging agents, RSC Adv. 6 (34) (2016) 28633–28639.

[27] X. Yang, Y. Zhuo, S. Zhu, Y. Luo, Y. Feng, Y. Dou, Novel and green synthesis of high-fluorescent carbon dots originated from honey for sensing and imaging, Biosens. Bioelectron. 60 (2014) 292–298.

[28] H. Xu, X. Yang, G. Li, C. Zhao, X. Liao, Green synthesis of fluorescent carbon dots for selective detection of tartrazine in food samples, J. Agric. Food Chem. 63 (30) (2015) 6707–6714, https://doi.org/10.1021/acs.jafc.5b02319.

[29] P. Das, M. Bose, S. Ganguly, S. Mondal, A.K. Das, S. Banerjee, N.C. Das, Green approach to photoluminescent carbon dots for imaging of Gram-negative bacteria Escherichia coli, Nanotechnology 28 (19) (2017), 195501. .

[30] C.-L. Li, C.-M. Ou, C.-C. Huang, W.-C. Wu, Y.-P. Chen, T.-E. Lin, L.-C. Ho, C.-W. Wang, C.-C. Shih, H.-C. Zhou, Y.-C. Lee, W.-F. Tzeng, T.-J. Chiou, S.-T. Chu, J. Cang, H.-T. Chang, Carbon dots prepared from ginger exhibiting efficient inhibition of human hepatocellular carcinoma cells, J. Mater. Chem. B 2 (28) (2014) 4564–4571, https://doi.org/10.1039/c4tb00216d.

[31] P.-C. Hsu, P.-C. Chen, C.-M. Ou, H.-Y. Chang, H.-T. Chang, Extremely high inhibition activity of photoluminescent carbon nanodots toward cancer cells, J. Mater. Chem. B 1 (13) (2013) 1774–1781.

[32] S.L. Banerjee, M. Khamrai, K. Sarkar, N.K. Singha, P.P. Kundu, Modified chitosan encapsulated core-shell Ag Nps for superior antimicrobial and anticancer activity, Int. J. Biol. Macromol. 85 (2016) 157–167, https://doi.org/10.1016/j.ijbiomac.2015.12.068.

[33] B. Moldovan, L. David, A. Vulcu, L. Olenic, M. Perde-Schrepler, E. Fischer-Fodor, I. Baldea, S. Clichici, G.A. Filip, In vitro and in vivo anti-inflammatory properties of green synthesized silver nanoparticles using Viburnum opulus L. fruits extract, Mater. Sci. Eng. C 79 (2017) 720–727, https://doi.org/10.1016/j.msec.2017.05.122.

[34] P. Sanpui, A. Chattopadhyay, S.S. Ghosh, Induction of apoptosis in cancer cells at low silver nanoparticle concentrations using chitosan nanocarrier, ACS Appl. Mater. Interfaces 3 (2) (2011) 218–228, https://doi.org/10.1021/am100840c.

[35] E. Zielinska, A. Zauszkiewicz-Pawlak, M. Wojcik, I. Inkielewicz-Stepniak, Silver nanoparticles of different sizes induce a mixed type of programmed cell death in human pancreatic ductal adenocarcinoma, Oncotarget 9 (4) (2018) 4675.

[36] B. Plackal Adimuriyil George, N. Kumar, H. Abrahamse, S.S. Ray, Apoptotic efficacy of multifaceted biosynthesized silver nanoparticles on human adenocarcinoma cells, Sci. Rep. 8 (1) (2018) 14368, https://doi.org/10.1038/s41598-018-32480-5.

[37] S. Kumar, S. Raj, K. Sarkar, K. Chatterjee, Engineering a multi-biofunctional composite using poly(ethylenimine) decorated graphene oxide for bone tissue regeneration, Nanoscale 8 (12) (2016) 6820–6836, https://doi.org/10.1039/C5NR06906H.

[38] Y.K. Jo, J.H. Seo, B.-H. Choi, B.J. Kim, H.H. Shin, B.H. Hwang, H.J. Cha, Surface-independent antibacterial coating using silver nanoparticle-generating engineered mussel glue, ACS Appl. Mater. Interfaces 6 (22) (2014) 20242–20253.

[39] Y. He, X. Li, Y. Zheng, Z. Wang, Z. Ma, Q. Yang, B. Yao, Y. Zhao, H. Zhang, A green approach for synthesizing silver nanoparticles, and their antibacterial and cytotoxic activities, New J. Chem. 42 (4) (2018) 2882–2888, https://doi.org/10.1039/C7NJ04224H.

[40] L. Zhao, F. Di, D. Wang, L.-H. Guo, Y. Yang, B. Wan, H. Zhang, Chemiluminescence of carbon dots under strong alkaline solutions: a novel insight into carbon dot optical properties, Nanoscale 5 (7) (2013) 2655–2658, https://doi.org/10.1039/C3NR00358B.

[41] Z. Yang, M. Xu, Y. Liu, F. He, F. Gao, Y. Su, H. Wei, Y. Zhang, Nitrogen-doped, carbon-rich, highly photoluminescent carbon dots from ammonium citrate, Nanoscale 6 (3) (2014) 1890–1895.

[42] J. Zhang, W. Shen, D. Pan, Z. Zhang, Y. Fang, M. Wu, Controlled synthesis of green and blue luminescent carbon nanoparticles with high yields by the carbonization of sucrose, New J. Chem. 34 (4) (2010) 591–593.

[43] K. Jyoti, M. Baunthiyal, A. Singh, Characterization of silver nanoparticles synthesized using Urtica dioica Linn. Leaves and their synergistic effects with antibiotics, J. Radiat. Res. Appl. Sci. 9 (3) (2016) 217–227.

[44] P. Das, K. Ghosal, N.K. Jana, A. Mukherjee, P. Basak, Green synthesis and characterization of silver nanoparticles using belladonna mother tincture and its efficacy as a potential antibacterial and anti-inflammatory agent, Mater. Chem. Phys. 228 (2019) 310–317.

[45] B. van Dam, H. Nie, B. Ju, E. Marino, J.M.J. Paulusse, P. Schall, M. Li, K. Dohnalová, Excitation-dependent photoluminescence from single-carbon dots, Small 13 (48) (2017), 1702098. https://doi.org/10.1002/smll.201702098.

[46] D. Yang, T. Li, M. Xu, F. Gao, J. Yang, Z. Yang, W. Le, Graphene oxide promotes the differentiation of mouse embryonic stem cells to dopamine neurons, Nanomedicine 9 (16) (2014) 2445–2455.

[47] A. Sachdev, I. Matai, P. Gopinath, Dual-functional carbon dots–silver@ zinc oxide nanocomposite: in vitro evaluation of cellular uptake and induction of apoptosis, J. Mater. Chem. B 3 (7) (2015) 1217–1229.

[48] S. Pal, Y.K. Tak, J.M. Song, Does the antibacterial activity of silver nanoparticles depend on the shape of the nanoparticle? A study of the Gram-negative bacterium Escherichia coli, Appl. Environ. Microbiol. 73 (6) (2007) 1712–1720.

[49] E. Arkan, A. Barati, M. Rahmanpanah, L. Hosseinzadeh, S. Moradi, M. Hajialyani, Green synthesis of carbon dots derived from walnut oil and an investigation of their cytotoxic and apoptogenic activities toward cancer cells, Adv. Pharm. Bull. 8 (1) (2018) 149.

[50] G. Huang, X. Chen, C. Wang, H. Zheng, Z. Huang, D. Chen, H. Xie, Photoluminescent carbon dots derived from sugarcane molasses: synthesis, properties, and applications, RSC Adv. 7 (75) (2017) 47840–47847.

[51] R. Bhanumathi, K. Vimala, K. Shanthi, R. Thangaraj, S. Kannan, Bioformulation of silver nanoparticles as berberine carrier cum anticancer agent against breast cancer, New J. Chem. 41 (23) (2017) 14466–14477.

[52] L. Salazar, M.J. Vallejo López, M. Grijalva, L. Castillo, A. Maldonado, Biological effect of organically coated Grias neuberthii and Persea americana silver nanoparticles on HeLa and MCF-7 cancer cell lines, J. Nanotechnol. 2018 (2018).

[53] Y.-g. Yuan, Q.-L. Peng, S. Gurunathan, Silver nanoparticles enhance the apoptotic potential of gemcitabine in human ovarian cancer cells: combination therapy for effective cancer treatment, Int. J. Nanomedicine 12 (2017) 6487.

[54] J.-K. Jeong, S. Gurunathan, M.-H. Kang, J.W. Han, J. Das, Y.-J. Choi, D.-N. Kwon, S.-G. Cho, C. Park, H.G. Seo, Hypoxia-mediated autophagic flux inhibits silver nanoparticle-triggered apoptosis in human lung cancer cells, Sci. Rep. 6 (2016), 21688. .

[55] Y. Suzuki-Karasaki, M. Suzuki-Karasaki, M. Uchida, T. Ochiai, Depolarization controls TRAIL-sensitization and tumor-selective killing of cancer cells: crosstalk with ROS, Front. Oncol. 4 (2014) 128.

[56] E. Barcińska, J. Wierzbicka, A. Zauszkiewicz-Pawlak, D. Jacewicz, A. Dabrowska, I. Inkielewicz-Stepniak, Role of oxidative and nitro-oxidative damage in silver nanoparticles cytotoxic effect against human pancreatic ductal adenocarcinoma cells, Oxidative Med. Cell. Longev. 2018 (2018).

[57] A. El-Hussein, M.R. Hamblin, ROS generation and DNA damage with photoinactivation mediated by silver nanoparticles in lung cancer cell line, IET Nanobiotechnol. 11 (2) (2016) 173–178.

[58] J.-C. Jin, Z.-Q. Xu, P. Dong, L. Lai, J.-Y. Lan, F.-L. Jiang, Y. Liu, One-step synthesis of silver nanoparticles using carbon dots as reducing and stabilizing agents and their antibacterial mechanisms, Carbon 94 (2015) 129–141, https://doi.org/10.1016/j.carbon.2015.05.084.

[59] S. Elmore, Apoptosis: a review of programmed cell death, Toxicol. Pathol. 35 (4) (2007) 495–516, https://doi.org/10.1080/01926230701320337.